Timing and climate forcing of volcanic eruptions for the past 2,500 years

Sigl, M., Winstrup, M., McConnell, J. R., Welten, K. C., Plunkett, G., Ludlow, F., Büntgen, U., Caffee, M., Chellman, N., Dahl-Jensen, D., Fischer, H., Kipfstuhl, S., Kostick, C., Maselli, O. J., Mekhaldi, F., Mulvaney, R., Muscheler, R., Pasteris, D. R., Pilcher, J. R., ... Woodruff, T. E. (2015). Timing and climate forcing of volcanic eruptions for the past 2,500 years. *Nature*, *523*(7562), 543–549. https://doi.org/10.1038/nature14565

Queen's University Belfast - Research Portal:
Link to publication record in Queen's University Belfast Research Portal

1   **Timing and climate forcing of volcanic eruptions for the past 2,500 years**

2

3   M. Sigl[1,2], M. Winstrup[3], J.R. McConnell[1], K.C. Welten[4], G. Plunkett[5], F. Ludlow[6], U. Büntgen[7,8,9], M.

4   Caffee[10,11], N. Chellman[1], D. Dahl-Jensen[12], H. Fischer[8,13], S. Kipfstuhl[14], C. Kostick[15], O.J. Maselli[1], F.

5   Mekhaldi[16], R. Mulvaney[17], R. Muscheler[16], D.R. Pasteris[1], J.R. Pilcher[5], M. Salzer[18], S. Schüpbach[8,13], J.P.

6   Steffensen[12], B.M. Vinther[12], T.E. Woodruff[10]

7

8   [1] Desert Research Institute, Nevada System of Higher Education, Reno, NV 89512, USA

9   [2] now at Laboratory of Radiochemistry and Environmental Chemistry, Paul Scherrer Institut, 5232 Villigen,
10   Switzerland

11   [3] Department of Earth and Space Sciences, University of Washington, Seattle, WA 98195, USA

12   [4] Space Sciences Laboratory, University of California, Berkeley, CA 94720, USA

13   [5] School of Geography, Archaeology & Palaeoecology, Queen's University Belfast, Belfast BT7 1NN, UK

14   [6] Yale Climate & Energy Institute, and Department of History, Yale University, New Haven, CT 06511, USA

15   [7] Swiss Federal Research Institute WSL, 8903 Birmensdorf, Switzerland

16   [8] Oeschger Centre for Climate Change Research, University of Bern, 3012 Bern, Switzerland

17   [9] Global Change Research Centre AS CR, 60300 Brno, Czech Republic

18   [10] Department of Physics, Purdue University, West Lafayette, IN 47907, USA

19   [11] Department of Earth, Atmospheric, and Planetary Sciences, Purdue University, West Lafayette, IN 47907,

20   USA

21   [12] Centre for Ice and Climate, Niels Bohr Institute, University of Copenhagen, 2100 Copenhagen, Denmark

22   [13] Climate and Environmental Physics, University of Bern, 3012 Bern, Switzerland

23   [14] Alfred-Wegener-Institut Helmholtz-Zentrum für Polar- und Meeresforschung, 27570 Bremerhaven, Germany

24   [15] Department of History, The University of Nottingham, Nottingham NG7 2RD, UK

25   [16] Department of Geology, Quaternary Sciences, Lund University, 22362 Lund, Sweden

26   [17] British Antarctic Survey, Natural Environment Research Council, Cambridge, CB3 0ET, UK

27   [18] The Laboratory of Tree-Ring Research, University of Arizona, Tucson, AZ 85721, USA

28

Volcanic eruptions contribute to climate variability, but quantifying these contributions has been limited by inconsistencies in the timing of atmospheric volcanic aerosol loading determined from ice cores and subsequent cooling from climate proxies such as tree rings. Using new records of atmospheric aerosol loading developed from high-resolution, multi-parameter measurements from an array of Greenland and Antarctic ice cores as well as distinctive age markers to constrain chronologies, we resolve these inconsistencies. Here we show that large eruptions in the tropics and high latitudes were primary drivers of interannual-to-decadal temperature variability in the Northern Hemisphere during the past 2,500 years. Overall, cooling was proportional to the magnitude of volcanic forcing and persisted for up to ten years after some of the largest eruptive episodes. Our revised timescale now firmly implicates volcanic eruptions as catalysts in the major 6th century pandemics, famines, and socioeconomic disruptions in Eurasia and Mesoamerica while allowing multi-millennium quantification of climate response to volcanic forcing.

Volcanic eruptions are primary drivers of natural climate variability – as sulfate aerosol injections into the stratosphere shield the Earth's surface from incoming solar radiation, leading to short-term cooling at regional-to-global scales[1]. Temperatures during the past 2,000 years have been reconstructed at regional[2], continental[3], and global scales[4] using proxy information from natural archives. Tree-ring-based proxies provide the vast majority of climate records from mid- to high-latitude regions of (predominantly) the Northern Hemisphere (NH), whereas ice-core records (e.g., $\delta^{18}O$) represent both polar regions[3]. Climate forcing reconstructions for the Common Era (CE) – including solar (e.g., ^{10}Be)[5] and volcanic (e.g., sulfate)[6,7] activity – mostly derive from ice-core proxies. Any attempt to attribute reconstructed climate variability to external volcanic forcing – and distinguish between response, feedback, and internal variability of the climate system – requires ice-core chronologies that are synchronous with those of other climate reconstructions. In addition, multi-proxy climate reconstructions[2-4] derived from ice cores and other proxies such as tree rings will have diminished high-to-mid-frequency amplitudes if the individual climate records are on different timescales. Magnitudes and relative timing of simulated NH temperature response to large volcanic

55 eruptions are in disagreement with reconstructed temperatures obtained from tree rings[8,9], but it is

56 unclear to what extent this model/data mismatch is caused by limitations in temperature

57 reconstructions, volcanic reconstructions, or implementation of aerosol forcing in climate models[9-11].

58 The hypothesis of chronological errors in tree-ring-based temperature reconstructions[8,9] offered to

59 explain this model/data mismatch has been tested and widely rejected[11-14], while new ice-core

60 records have become available providing different eruption ages[15,16] and more precise estimates of

61 atmospheric aerosol mass loading[17] than previous volcanic reconstructions. Using documented[18] and

62 previous ice-core-based eruption ages[16], strong summer cooling following large volcanic eruptions

63 has been recorded in tree-ring-based temperature reconstructions during the 2nd millennium CE with

64 a one-to-two year lag similar to that observed in instrumental records after the 1991 Pinatubo

65 eruption[19]. An apparent seven-year delayed cooling observed in individual tree-ring series relative to

66 Greenland ice-core acidity peaks during the 1st millennium CE, however, suggests a bias in existing

67 ice-core chronologies[20,21]. Using published ice-core chronologies, we also observed a seven-year

68 offset between sulfate deposition in North Greenland and the start of tree-ring growth reduction in

69 a composite of five multi-centennial tree-ring summer temperature reconstructions ("N-Tree") from

70 the NH between 1 and 1000 CE (Methods), whereas tree-ring response was effectively immediate

71 for eruptions occurring after 1250 CE (Fig. 1a).

72 **Precise time marker across hemispheres.** Independent age markers to test the accuracy of tree-ring

73 and ice-core chronologies recently have become available with the detection of abrupt enrichment

74 events in the ^{14}C content of tree rings. Rapid increases of atmospheric ^{14}C were first identified in

75 individual growth increments of cedars from Japan between 774 and 775 CE[22] and between 993 and

76 994 CE[23]. The presence and timing of the event in 775 CE (henceforth, 775 event) has been

77 reproduced by all radiocarbon measurements performed on tree rings at annual (or higher)

78 resolution – including tree cores from Germany[24], the Alps[12], the Great Basin[25] (USA), and Siberia[25].

79 Recent identification of the same 775 CE event in kauri wood samples from New Zealand in the

80 Southern Hemisphere (SH) demonstrates the global extent of the rapid ^{14}C increase and provides

81   further constraints on the event's exact timing (March 775 ± 6 months) due to the asynchronous SH

82   growing season[26]. While the cause of the 775 and 994 events is still debated[22,24,27], we expect that

83   they might also produce an excess of cosmogenic [10]Be through the interaction of high-energy

84   particles with atmospheric constituents[28,29]. Since both of these radionuclides are incorporated

85   rapidly into proxy archives via aerosol deposition ([10]Be in ice cores) and photosynthesis ([14]CO_2 in tree

86   rings), isotopic anomalies caused by these extraterrestrial events provide a global age marker to

87   directly link ice-core records to tree-ring chronologies[27]. The latter serve as an absolute and precise

88   age marker, verified (at least since 775 CE) by the coherence of the rapid increase in ^{14}C in all tree-

89   rings records for which high-resolution radiocarbon analyses were performed, including those

90   speculated to be at risk of missing rings[8]. We measured [10]Be concentrations at approximately annual

91   resolution in four ice cores – NEEM-2011-S1, TUNU2013, and NGRIP in Greenland, and the West

92   Antarctic Ice Sheet Divide Core (WDC) – over depth ranges encompassing the year 775 as dated in

93   existing ice-core chronologies in order to provide a direct, physically-based test of any dating bias in

94   these chronologies (Fig. 1, Extended Data Fig. 1, Methods, Supplementary Data S1). Both polar ice

95   sheets contain [10]Be concentrations exceeding the natural background concentration (>150%; 6σ) for

96   one-to-two consecutive years, compatible with the 775 CE event observed in tree rings. Using the

97   original ice-core age models[16,30], the ages of the [10]Be maxima in NEEM-2011-S1, NGRIP, and WDC are

98   768 CE, offset by 7 years from the tree-ring event. A further [10]Be anomaly measured in NEEM-2011-

99   S1 at 987 CE, compatible with the 994 CE event in tree rings, suggests a chronological offset was

100   present by the end of the first millennium CE (Fig. 1). Several different causes may have contributed

101   to the offset (see a summary in the Methods section), among which is the use of a previous dating

102   constraint[30] for Greenland where volcanic fallout in the ice was believed to indicate the historic (79

103   CE) eruption of Vesuvius.

104   **Revised ice-core chronologies.** Given the detection of a bias in existing ice-core chronologies, we

105   developed new timescales prior to the 1257 Samalas eruption[31] using highly resolved, multi-

106   parameter aerosol concentration records from three ice cores: NEEM-2011-S1, NEEM, and WDC. We

107   used the StratiCounter program, an automated, objective, annual-layer detection method based on

108   Hidden Markov Model (HMM) algorithms[32] (Methods). For NEEM-2011-S1, obtained confidence

109   intervals for the layer counts allowed us to improve the dating further by constraining the timescale

110   using the 775 CE ^{10}Be anomaly and three precisely dated observations of post-volcanic aerosol

111   loading of the atmosphere (Fig. 2, Extended Data Tables 1-3, Methods, Supplementary Data S2). We

112   evaluated the accuracy of our new chronologies ("WD2014" for WDC and "NS1-2011" for NEEM) by

113   comparison to (1) an extensive database of historical volcanic dust veil observations (Extended Data

114   Fig. 2, Methods, Supplementary Data S2), (2) ice-core tephra evidence (Methods), and (3) the 994 CE

115   event (Methods, Fig. 2). Using the new timescales, we found large sulfate signals in Greenland (e.g.

116   682, 574, 540 CE) between 500 and 2000 CE that frequently occurred within ±1 year from

117   comparable – and independently dated – signals in Antarctica. These bipolar signals can now be

118   confidently attributed to large tropical eruptions (Fig. 2). Back to 400 BCE, other large sulfate peaks

119   (e.g., 44 BCE) were synchronous to within ±3 years (Fig. 2). We conclude that the revised ice-core

120   timescales are accurate to within less than ±5 years during the past 2,500 years based on combined

121   evidence from radionuclides, tree rings, tephra analyses, and historical accounts. Compared to the

122   previous chronologies, age models differ prior to 1250 CE by up to 11 years (GICC05, Greenland) and

123   14 years (WDC06A-7, Antarctica) (Extended Data Fig. 3).

124   **History of volcanic forcing.** Employing our revised timescales and new high-resolution, ice-core

125   sulfur measurements, we developed an extended reconstruction of volcanic aerosol deposition since

126   early Roman times for both polar ice sheets from which we then estimated radiative forcing using

127   established transfer functions[15] (Fig. 3, Methods, Supplementary Data S3-S5). This forcing series is

128   characterized by improved dating accuracy, annual resolution, and a larger number of ice-core

129   records in the Antarctic ice-core sulfate composite[17] than previous reconstructions[6,7]. It spans 2,500

130   years, allowing investigation of climate-volcano linkages more accurately and earlier than with

131   previous reconstructions. It also provides a perspective on volcanic influences during major historical

132   epochs, such as the growth of Roman imperial power and subsequent decline of the migration

133 period in Europe – times of (1) demographic and economic expansion as well as relative societal

134 stability and (2) political turmoil and population instability, respectively[33]. With improved dating and

135 lower volcanic-sulfate detection limits from the Antarctic array[17], we were able to detect, estimate,

136 and attribute volcanic aerosol loading and forcing from 283 individual eruptive events during this

137 period (Fig. 3). We attributed about 50% to mid-to-high latitudes NH sources, while 81 were

138 attributed to tropical eruptions (having synchronous sulfate deposition on both polar ice sheets).

139 These tropical volcanic eruptions contributed 64% of total volcanic forcing throughout the period,

140 with five events exceeding the sulfate loading from Tambora, 1815 (Fig. 3, Extended Data Table 4).

141 Events in 426 BCE and 44 BCE rival the great 1257 CE Samalas eruption (Indonesia) as the largest

142 sulfate producing eruptions during this time. These two earlier events have not been widely

143 regarded as large tropical eruptions with potential for strong climate impact[20], due to the lack of

144 complete and synchronized sulfate records from Greenland and Antarctica. We base the claim that

145 these two eruptions were tropical in origin and caused significant radiative perturbations on the

146 observation that ice cores from Greenland and Antarctica record coeval (within their respective age

147 uncertainties) and exceptionally high volcanic sulfate concentrations. Both these events were

148 followed by strong and persistent growth reduction in tree-ring records[34] (Fig. 2) as typically

149 observed after large tropical eruptions during the Common Era (Fig. 3).

150 **Post-volcanic summer cooling.** Superposed epoch analyses (Methods) performed on the "N-Tree"

151 composite record centered on the largest volcanic signals between 500 BCE and 1250 CE as well as

152 between 1250 and 2000 CE, show a clear post-volcanic cooling signal. For both periods, maximum

153 tree-ring response lagged the date of initial increase of sulfate deposition by one year (Fig. 2),

154 consistent with the response observed if using only historically documented eruptions with secure

155 dating for the past 800 years[18]. The sharp and immediate (i.e., ≤1 year lag) response of tree growth

156 to the ice-core volcanic signal throughout the past 2,500 years further corroborates the accuracy of

157 our new ice-core timescales (Extended Data Fig. 4). Of the 16 most negative tree-growth anomalies

158 (i.e., coldest summers) between 500 BCE and 1000 CE, 15 followed large volcanic signals – with the

159　four coldest (43 BCE, 536, 543, and 627 CE) occurring shortly after several of the largest events

160　(Extended Data Tables 4, 5). Similarly, the coldest summers in Europe during the Common Era[3] were

161　associated with large volcanic eruptions (Extended Data Table 5). Reduced tree growth after volcanic

162　eruptions also was prominent in decadal averages of the "N-Tree" composite. All 16 decades with

163　the most reduced tree growth for our 2,500-year period followed large eruptions (Fig. 3, Extended

164　Data Table 5). In many cases, such as the coldest decade from 536 to 545 CE[3], sustained cooling was

165　associated with the combined effect of several successive volcanic eruptions.

166　　　Strong post-volcanic cooling was not restricted to tropical eruptions; it also followed NH

167　eruptions (Fig. 4), with maximum cooling in the year of volcanic-sulfate deposition. In contrast to the

168　average of the 19 largest CE tropical eruptions, however, the NH-only eruptions did not give rise to

169　any significant long-term cooling effect (Fig. 4). Persistence of implied post-volcanic cooling following

170　the largest tropical eruptions is strongly expressed in temperature reconstructions based on tree-

171　ring width measurements (e.g., those from the Alps), with recovery times of more than 10 years.

172　Persistent cooling, with temperature reduction significantly below the pre-eruption baseline for six

173　consecutive years, also is observed in temperature reconstructions based on maximum latewood

174　density (e.g., those from Northern Scandinavia), the preferred proxy to quantify volcanic cooling

175　contributions on climate due to less marked biological memory effects[35] (Fig. 4). These findings

176　indicate that eruption-induced climate anomalies following large tropical eruptions may last longer

177　than is indicated in many climate simulations (<3–5 years)[9,36,37] and that potential positive feedbacks

178　initiated after large tropical eruptions (e.g., sea-ice feedbacks) may not be adequately represented in

179　climate simulations[38,39]. The five-year averaged (lag 0 to lag 4 years) cooling response over three NH

180　regions (Methods) following the 19 largest CE tropical eruptions was -0.6 ± 0.2 °C (2 standard error

181　of the mean (SEM)), that of large NH eruptions was -0.4 ± 0.4 °C with strongest cooling induced in

182　the high latitudes. Overall, cooling was proportional to the magnitude of volcanic forcing, with

183　stratospheric sulfate loading exceeding that of Tambora inducing the strongest response of -1.1 ±

184　0.6 °C (Figs. 3, 4).

185 **Global climate anomalies in 536-550 CE.** Our new dating allowed us to clarify long-standing debates

186 concerning the origin and consequences of the severe and apparently global climate anomalies

187 observed from c.536–550 CE, which began with recognition of the "mystery cloud" of 536 CE[40]

188 observed in the Mediterranean basin. Under previous ice-core dating, it has been argued that this

189 dust veil corresponded to an unknown tropical eruption dated 533–534 CE (±2)[41]. Using our revised

190 timescales, we found at least two large volcanic eruptions around this period (Fig. 5). A first –

191 apparently NH, eruptive episode in 535 or early 536 CE – injected large amounts of sulfate and ash

192 into the atmosphere. Geochemistry of tephra filtered from the NEEM-2011-S1 ice core at a depth

193 corresponding to 536 CE indicated multiple North American volcanoes as likely candidates for a

194 combined volcanic signal (Extended Data Fig. 5, Methods, Supplementary Data S5). Historical

195 observations (Extended Data Table 3) identified atmospheric dimming as early as March 24, 536,

196 lasting up to 18 months. The summer of 536 CE appeared exceptionally cold in all tree-ring

197 reconstructions in the extra-tropical NH from N-America[34], over Europe[35,42,43] to Asia[44]. Depending

198 upon reconstruction method, European summer temperatures in 536 CE dropped 1.6-2.5°C relative

199 to the previous 30-year average[3]. A second eruptive episode in 539 or 540 CE, identified in both

200 Greenland and Antarctica ice-core records and hence likely tropical in origin, resulted in up to 10%

201 higher global aerosol loading than the Tambora 1815 eruption reconstructed from our bipolar

202 sulfate records. Summer temperatures consequently dropped again, by 1.4-2.7°C in Europe in 541

203 CE[3], and cold temperatures persisted in the NH until almost 550 CE[3,33,34,42] (Figs. 2, 3, 5). This

204 provides a notable environmental context to widespread famine and the great Justinian Plague 541-

205 543 CE that was responsible for decimating populations in the Mediterranean and potentially

206 China[45,46]. While certain climatic conditions (e.g., wet summers) have been linked to plague

207 outbreaks in the past[47], a direct causal connection of these two large volcanic episodes and

208 subsequent cooling to crop failures and outbreaks of famines and plagues is difficult to prove[33].

209 However, the exact delineation of two of the largest volcanic signals – with exceptionally strong and

210 prolonged NH cooling; written evidence of famines and pandemics; as well as socio-economic

211 decline observed in Mesoamerica ("Maya Hiatus"[48]), Europe, and Asia – supports the idea that the

212 latter may be causally associated with volcanically-induced climatic extremes.

213   Detailed study of major volcanic events during the 6th century (Fig. 5) and an assessment of post-

214 volcanic cooling throughout the past 2,500 years using stacked tree-ring records and regional

215 temperature reconstructions (Fig. 4, Extended Data Fig. 4) demonstrated that large eruptions in the

216 tropics and high latitudes were primary drivers of interannual-to-decadal NH temperature variability.

217 The new ice-core chronologies imply that previous multi-proxy reconstructions of temperature that

218 include ice-core records[2-4] have diminished high-to-mid-frequency amplitudes and must be updated

219 to accurately capture the timing and full amplitude of paleoclimatic variability. By creating a volcanic

220 forcing index independent of but consistent with tree-ring-indicated cooling, we provide an essential

221 step to advance understanding of external forcing on natural climate variability during the past 2,500

222 years. With the expected detection of additional rapid Δ^{14}C enrichment events from ongoing efforts

223 in annual resolution ^{14}C tree-ring analyses[49], there will be future opportunities to further constrain

224 ice-core dating throughout the Holocene and develop a framework of precisely dated, globally

225 synchronized proxies of past climate variability and external climate forcing.

226 1   Robock, A. Volcanic eruptions and climate. *Rev Geophys* **45**, doi: 1029/2007rg000232 (2007).

227 2   Hanhijarvi, S., Tingley, M. P. & Korhola, A. Pairwise comparisons to reconstruct mean

228   temperature in the Arctic Atlantic Region over the last 2,000 years. *Clim Dynam* **41**, 2039-

229   2060 (2013).

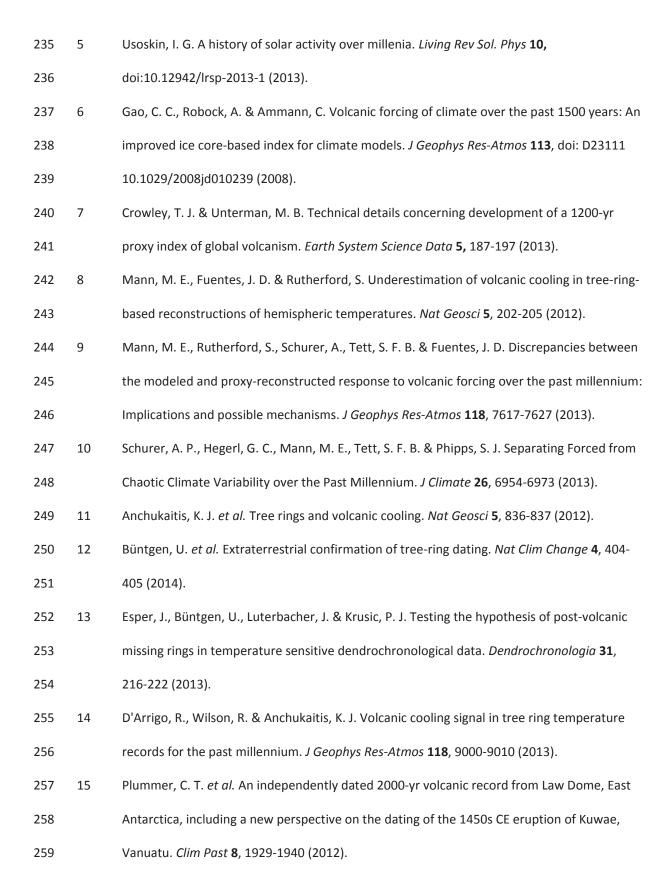230 3   PAGES 2k Consortium Continental-scale temperature variability during the past two

231   millennia. *Nature Geoscience* **6**, doi: 10.1038/Ngeo1834 (2013).

232 4   Mann, M. E. *et al.* Proxy-based reconstructions of hemispheric and global surface

233   temperature variations over the past two millennia. *P Natl Acad Sci USA* **105**, 13252-13257,

234   (2008).

235   5   Usoskin, I. G. A history of solar activity over millenia. *Living Rev Sol. Phys* **10,**

236   doi:10.12942/lrsp-2013-1 (2013).

237   6   Gao, C. C., Robock, A. & Ammann, C. Volcanic forcing of climate over the past 1500 years: An

238   improved ice core-based index for climate models. *J Geophys Res-Atmos* **113**, doi: D23111

239   10.1029/2008jd010239 (2008).

240   7   Crowley, T. J. & Unterman, M. B. Technical details concerning development of a 1200-yr

241   proxy index of global volcanism. *Earth System Science Data* **5,** 187-197 (2013).

242   8   Mann, M. E., Fuentes, J. D. & Rutherford, S. Underestimation of volcanic cooling in tree-ring-

243   based reconstructions of hemispheric temperatures. *Nat Geosci* **5**, 202-205 (2012).

244   9   Mann, M. E., Rutherford, S., Schurer, A., Tett, S. F. B. & Fuentes, J. D. Discrepancies between

245   the modeled and proxy-reconstructed response to volcanic forcing over the past millennium:

246   Implications and possible mechanisms. *J Geophys Res-Atmos* **118**, 7617-7627 (2013).

247   10   Schurer, A. P., Hegerl, G. C., Mann, M. E., Tett, S. F. B. & Phipps, S. J. Separating Forced from

248   Chaotic Climate Variability over the Past Millennium. *J Climate* **26**, 6954-6973 (2013).

249   11   Anchukaitis, K. J. *et al.* Tree rings and volcanic cooling. *Nat Geosci* **5**, 836-837 (2012).

250   12   Büntgen, U. *et al.* Extraterrestrial confirmation of tree-ring dating. *Nat Clim Change* **4**, 404-

251   405 (2014).

252   13   Esper, J., Büntgen, U., Luterbacher, J. & Krusic, P. J. Testing the hypothesis of post-volcanic

253   missing rings in temperature sensitive dendrochronological data. *Dendrochronologia* **31**,

254   216-222 (2013).

255   14   D'Arrigo, R., Wilson, R. & Anchukaitis, K. J. Volcanic cooling signal in tree ring temperature

256   records for the past millennium. *J Geophys Res-Atmos* **118**, 9000-9010 (2013).

257   15   Plummer, C. T. *et al.* An independently dated 2000-yr volcanic record from Law Dome, East

258   Antarctica, including a new perspective on the dating of the 1450s CE eruption of Kuwae,

259   Vanuatu. *Clim Past* **8**, 1929-1940 (2012).

260   16   Sigl, M. *et al.* A new bipolar ice core record of volcanism from WAIS Divide and NEEM and

261   implications for climate forcing of the last 2000 years. *J Geophys Res-Atmos* **118**, 1151-1169

262   (2013).

263   17   Sigl, M. *et al.* Insights from Antarctica on volcanic forcing during the Common Era. *Nat Clim*

264   *Change* **4**, 693-697 (2014).

265   18   Esper, J. *et al.* European summer temperature response to annually dated volcanic eruptions

266   over the past nine centuries. *B Volcanol* **75**, doi: 10.1007/S00445-013-0736-Z (2013).

267   19   Douglass, D. H. & Knox, R. S. Climate forcing by the volcanic eruption of Mount Pinatubo.

268   *Geophys Res Lett* **32**, L05710, doi: 10.1029/2004gl022119 (2005).

269   20   Baillie, M. G. L. Proposed re-dating of the European ice core chronology by seven years prior

270   to the 7th century AD. *Geophys Res Lett* **35**, L15813, doi: 10.1029/2008gl034755 (2008).

271   21   Baillie, M. G. L. & McAneney, J. Tree ring effects and ice core acidities clarify the volcanic

272   record of the 1st millennium. *Clim. Past* **11**, 105-114 (2015).

273   22   Miyake, F., Nagaya, K., Masuda, K. & Nakamura, T. A signature of cosmic-ray increase in AD

274   774-775 from tree rings in Japan. *Nature* **486**, 240-242 (2012).

275   23   Miyake, F., Masuda, K. & Nakamura, T. Another rapid event in the carbon-14 content of tree

276   rings. *Nat Commun* **4**, doi: 10.1038/Ncomms2783 (2013).

277   24   Usoskin, I. G. *et al.* The AD775 cosmic event revisited: the Sun is to blame. *Astron Astrophys*

278   **552**, doi: 10.1051/0004-6361/201321080 (2013).

279   25   Jull, A. J. T. *et al.* Excursions in the 14C record at A. D. 774-775 in tree rings from Russia and

280   America. *Geophys Res Lett* **41**, 3004-3010 (2014).

281   26   Güttler, D. *et al.* Rapid increase in cosmogenic 14C in AD 775 measured in New Zealand kauri

282   trees indicates short-lived increase in 14C production spanning both hemispheres. *Earth*

283   *Planet. Sci. Lett.* **411**, 290-297 (2015).

284   27   Miyake, F. *et al.* Cosmic ray event of AD 774-775 shown in quasi-annual 10 Be data from the

285   Antarctic Dome Fuji ice core. *Geophys. Res. Lett.* **42**, 84-89 (2015).

286 28 Webber, W. R., Higbie, P. R. & McCracken, K. G. Production of the cosmogenic isotopes H-3,

287 Be-7, Be-10, and Cl-36 in the Earth's atmosphere by solar and galactic cosmic rays. *J Geophys*

288 *Res-Space* **112**, A10106, doi: 10.1029/2007ja012499 (2007).

289 29 Masarik, J. & Beer, J. An updated simulation of particle fluxes and cosmogenic nuclide

290 production in the Earth's atmosphere. *J Geophys Res-Atmos* **114**, D11103, doi:

291 10.1029/2008jd010557 (2009).

292 30 Vinther, B. M. *et al.* A synchronized dating of three Greenland ice cores throughout the

293 Holocene. *J Geophys Res-Atmos* **111**, D13102, doi: 10.1029/2005jd006921 (2006).

294 31 Lavigne, F. *et al.* Source of the great A.D. 1257 mystery eruption unveiled, Samalas volcano,

295 Rinjani Volcanic Complex, Indonesia. *P Natl Acad Sci USA* **110**, 16742-16747 (2013).

296 32 Winstrup, M. *et al.* An automated approach for annual layer counting in ice cores. *Clim Past*

297 **8**, 1881-1895 (2012).

298 33 McCormick, M. *et al.* Climate Change during and after the Roman Empire: Reconstructing

299 the Past from Scientific and Historical Evidence. *J Interdiscipl Hist* **43**, 169-220 (2012).

300 34 Salzer, M. W. & Hughes, M. K. Bristlecone pine tree rings and volcanic eruptions over the last

301 5000 yr. *Quaternary Res* **67**, 57-68 (2007).

302 35 Esper, J., Duthorn, E., Krusic, P. J., Timonen, M. & Buntgen, U. Northern European summer

303 temperature variations over the Common Era from integrated tree-ring density records. *J*

304 *Quaternary Sci* **29**, 487-494 (2014).

305 36 Crowley, T. J. Causes of climate change over the past 1000 years. *Science* **289**, 270-277

306 (2000).

307 37 Driscoll, S., Bozzo, A., Gray, L. J., Robock, A. & Stenchikov, G. Coupled Model

308 Intercomparison Project 5 (CMIP5) simulations of climate following volcanic eruptions. *J*

309 *Geophys Res-Atmos* **117**, D17105, doi: 10.1029/2012jd017607 (2012).

310 38 Schneider, D. P., Ammann, C. M., Otto-Bliesner, B. L. & Kaufman, D. S. Climate response to

311   large, high-latitude and low-latitude volcanic eruptions in the Community Climate System

312   Model. *J Geophys Res-Atmos* **114**, D15101, doi: 10.1029/2008jd011222 (2009).

313 39 Zanchettin, D. *et al.* Inter-hemispheric asymmetry in the sea-ice response to volcanic forcing

314   simulated by MPI-ESM (COSMOS-Mill). *Earth Syst Dynam* **5**, 223-242 (2014).

315 40 Stothers, R. B. Mystery Cloud of Ad-536. *Nature* **307**, 344-345 (1984).

316 41 Larsen, L. B. *et al.* New ice core evidence for a volcanic cause of the AD 536 dust veil.

317   *Geophys Res Lett* **35**, L04708, doi: 10.1029/2007gl032450 (2008).

318 42 Büntgen, U. *et al.* 2500 Years of European Climate Variability and Human Susceptibility.

319   *Science* **331**, 578-582 (2011).

320 43 Esper, J. *et al.* Orbital forcing of tree-ring data. *Nat Clim Change* **2**, 862-866 (2012).

321 44 D'Arrigo, R. *et al.* 1738 years of Mongolian temperature variability inferred from a tree-ring

322   width chronology of Siberian pine. *Geophys Res Lett* **28**, 543-546 (2001).

323 45 Zhang, Z. B. *et al.* Periodic climate cooling enhanced natural disasters and wars in China

324   during AD 10-1900. *P Roy Soc B-Biol Sci* **277**, 3745-3753 (2010).

325 46 Stothers, R. B. Volcanic dry fogs, climate cooling, and plague pandemics in Europe and the

326   Middle East. *Climatic Change* **42**, 713-723 (1999).

327 47 Stenseth, N. C. *et al.* Plague dynamics are driven by climate variation. *P Natl Acad Sci USA*

328   **103**, 13110-13115 (2006).

329 48 Dull, R. A. Evidence for forest clearance, agriculture, and human-induced erosion in

330   Precolumbian El Salvador. *Ann Assoc Am Geogr* **97**, 127-141 (2007).

331 49 Taylor, R. E. & Southon, J. Reviewing the Mid-First Millennium BC C-14 "warp" using C-

332   14/bristlecone pine data. *Nucl Instrum Meth B* **294**, 440-443 (2013).

333

334 **Supplementary Information** is available in the online version of the paper.

364   **Author Contributions.** M.Si. designed the study with input from J.R.M., M.W., G.P., and F.L. The

365   manuscript was written by M.Si., M.W., F.L., and J.R.M., with contributions from K.C.W., G.P., U.B.,

366   B.V. in interpretation of the measurements. Ice-core chemistry measurements were performed by

367   J.R.M., M.Si., O.J.M., N.C., D.R.P. (NEEM, B40, TUNU2013), and by S.S., H.F., R.Mul. (NEEM). K.C.W.,

368   T.E.W., and M.C. completed ice core [10]Be measurements. F.M. and R.Mus. were responsible for the

369   NGRIP ice core [10]Be measurements. M.Si., M.W., B.V., and J.R.M. analyzed ice-core data and

370   developed age models. F.L. and C.K. analyzed historical documentary data. G.P and J.R.P. performed

371   ice-core tephra analysis and data interpretation. U.B. and M.Sa. contributed tree-ring data. D.D.-J.,

372   B.V., J.P.S., S.K., and O.J.M. were involved in drilling of the NEEM ice core. TUNU2013 was drilled by

373   M.Si., N.C. and O.J.M., and the B40 ice core was drilled by S.K. and made available for chemistry

374   measurements. D.D.-J. and J.P.S. were responsible for NEEM project management, sample

375   distribution, logistics support, and management. All authors contributed toward improving the final

376   manuscript.

377   **Author Information.** The authors declare no competing financial interests. Correspondence and

378   requests for materials should be addressed to J.R.M. (Joe.McConnell@dri.edu).

379   **Figure 1 | Annual [10]Be ice-core records and post-volcanic cooling from tree rings under existing ice-**

380   **core chronologies. a)** Superposed epoch analysis for the seven largest volcanic signals in NEEM-

381   2011-S1 between 78 and 1000 CE and for the 10 largest eruptions between 1250 and 2000 CE,

382   respectively[16]. Shown are growth anomalies from a multi-centennial, temperature-sensitive tree-ring

383   composite (N-Tree[42,43,76-78], Methods) 10 years after the year of volcanic sulfate deposition at NEEM

384   ice core site in Greenland (GICC05 timescale), relative to the level five years prior to sulfate

385   deposition; **b)** annually resolved [10]Be concentration records from WDC, TUNU2013, NGRIP, and

386 NEEM-2011-S1 ice cores on their original timescales and annually resolved Δ^{14}C series from tree-ring

387 records between 755-795 CE[22,24], with arrows representing the suggested time shifts for

388 synchronization; error bars are 1σ measurement uncertainties; estimated relative age uncertainty

389 for TUNU2013 at this depth interval from volcanic synchronization with NEEM-2011-S1 is ±1 year; **c)**

390 annually resolved ^{10}Be concentration record from NEEM-2011-S1 ice core on its original timescale

391 and annually resolved Δ^{14}C series from tree rings between 980-1010 CE[23]; error bars are 1σ

392 measurement uncertainties.

393 **Figure 2 | Re-dated ice-core, non-sea-salt sulfur records from Greenland and Antarctica in relation**

394 **to growth anomalies in the N-Tree composite. a)** Upper panel: Ice-core, non-sea-salt sulfur (nssS)

395 records from Greenland (NEEM, NEEM-2011-S1) on the NS1-2011 timescale between 500 BCE and

396 1300 CE, with identified layer of Tianchi tephra[67] highlighted (orange star). Calendar years are given

397 for the start of volcanic sulfate deposition. Events used as fixed age markers to constrain the dating

398 (i.e., 536, 626, 775, 939, and 1258) are indicated (purple stars). Annually resolved ^{10}Be concentration

399 record (green) from NEEM-2011-S1 encompassing the two Δ^{14}C excursion events in trees from 775

400 and 994; middle panel: tree-ring growth anomalies (relative to 1000-1099 CE) for the N-Tree

401 composite[42,43,76-78]; lower panel: nssS records from Antarctica (WDC, B40) on the WD2014 timescale

402 and annually resolved ^{10}Be concentrations from WDC; **b)** superposed epoch analysis for 28 large

403 volcanic signals during the past 2,500 years. Tree-ring growth anomalies relative to the timing of

404 reconstructed sulfate deposition in Greenland (NS1-2011) are shown for 1250 to 2000 CE and 500

405 BCE to 1250 CE.

406 **Figure 3 | Global volcanic aerosol forcing and NH temperature variations for the past 2,500 years.**

407 **a)** 2,500 year record of tree-growth anomalies (N-Tree[42,43,76-78]; relative to 1000-1099 CE) and

408 reconstructed summer temperature anomalies for Europe and Arctic[3] ; 40 coldest single years and

409 12 coldest decades based on N-Tree are indicated; **b)** reconstructed global volcanic aerosol forcing

410 from bipolar sulfate composite records from tropical (bipolar), NH, and SH eruptions. Total (i.e., time

411   integrated) forcing values are calculated by summing the annual values for the duration of volcanic

412   sulfur deposition. 40 largest volcanic signals are indicated, and ages are given for events

413   representing atmospheric sulfate loading exceeding Tambora 1815.

414   **Figure 4 | Post-volcanic cooling.** Superposed composites (time segments from selected periods in

415   the Common Era positioned so that the years with peak negative forcing are aligned) of the JJA

416   temperature response to: **a)-c)** 24 largest eruptions (>Pinatubo 1991) for three regional

417   reconstructions in Europe[3,35,42]; **d)-f)** 19 largest tropical eruptions; **g)** five largest NH eruptions; **h)**

418   eruptions with negative forcing larger than Tambora 1815 for Northern Europe and **i)** for Central

419   Europe (note the different scale for g-i); shown are JJA temperature anomalies (°C) for 15 years after

420   reconstructed volcanic peak forcing, relative to the five years before the volcanic eruption. Dashed

421   lines present two times the standard error of the mean (2 SEM) of the temperature anomalies

422   associated with the multiple eruptions. 5-year average post-volcanic temperatures are shown for

423   each reconstruction (lag 0 to lag +4 yrs, gray shading).

424   **Figure 5 | Volcanism and temperature variability during the Migration Period (500-705 CE).** Upper

425   panel: Ice-core non-sea-salt sulfur (nssS) records from Greenland (NEEM-2011-S1, TUNU2013).

426   Insets give translations of historical documents describing observation of post-volcanic atmospheric

427   effects in 536-537 and 626-627 CE. Calendar years for five large eruptions are given for the start of

428   volcanic sulfate deposition; middle panel: Summer temperature anomalies for Europe[3], and

429   reconstructed N-Tree growth anomalies and occurrence of frost rings in North American bristlecone

430   pine tree-ring records; lower panel: nssS records from Antarctica (WDC, B40) on the WD2014

431   timescale; attribution of the sulfur signals to bipolar, NH, and SH events based on the timing of

432   deposition on the two independent timescales is indicated by shading.

433   **Methods**

434   **Ice cores.** This study included new and previously described ice-core records from five drilling sites

435   (Extended Data Fig. 1, Supplementary Data S1). The upper 577 m of the 3,405 m WAIS Divide (WDC)

436   core from central West Antarctica and a 410 m intermediate-length core (NEEM-2011-S1) drilled in

437   2011 close to the 2,540 m North Greenland Eemian Ice Drilling (NEEM)[50] ice core previously have

438   been used to reconstruct sulfate deposition in both polar ice sheets[16]. These coring sites are

439   characterized by relatively high snowfall (~200 kg m^{-2} yr^{-1}) and have comparable elevation, latitude,

440   and deposition regimes. WDC and NEEM-2011-S1 provided high-resolution records that allowed

441   annual-layer dating based on seasonally varying impurity content[16]. New ice-core analyses included

442   the upper 514 m of the main NEEM core used to extend the record of NEEM-2011-S1 to cover the

443   past 2,500 years, as well as B40 drilled in 2012 in Dronning Maud Land in East Antarctica and

444   TUNU2013 drilled in 2013 in Northeast Greenland – both characterized by lower snowfall rates (~70-

445   100 kg m^{-2} yr^{-1}). Volcanic sulfate concentration from B40 had been reported previously for the past

446   2,000 years[17], but we extended measurements to 200 m depth to cover the past 2,500 years.

447   **High-resolution, ice-core aerosol analyses.** Ice-core analyses were performed at the Desert

448   Research Institute (DRI) using 55 to 100 cm long, longitudinal ice core sections (33 x 33 mm wide).

449   The analytical system for continuous analysis included two Element2 (Thermo Scientific) high-

450   resolution inductively coupled plasma mass spectrometers (HR-ICP-MS) operating in parallel for

451   measurement of a broad range of ~35 elements; an SP2 (Droplet Measurement Technologies)

452   instrument for black carbon (BC) measurements; and a host of fluorimeters and spectrophotometers

453   for ammonium (NH_4^+), nitrate (NO_3^-), hydrogen peroxide (H_2O_2), and other chemical species. All

454   measurements were exactly co-registered in depth, with depth resolution typically less than 10-15

455   mm[51-53]. We corrected total sulfur (S) concentrations for the sea-salt-sulfur contribution using sea-

456   salt-Na concentrations[16]. Measurements included TUNU2013 and NEEM (400-515 m) in Greenland,

457   and B40 in Antarctica (Extended Data Fig. 1). Gaps (i.e., ice not allocated to DRI) in the high-

458   resolution sulfur data of the NEEM core were filled with ~4 cm resolution discrete sulfate

459   measurements using fast ion-chromatography techniques[54] performed in the field between 428 and

460   506 m depth.

461   Independent analyses of the upper part of the NEEM main core were performed in the field

462   using a continuous flow analysis (CFA) system[55] recently modified to include a new melter head

463   design[56]. Ca^{2+}, NH_4^+, and H_2O_2 were analyzed by fluorescence spectroscopy; Na^+ and NO_3^- by

464   absorption spectroscopy; conductivity of the meltwater by a micro flow cell (Amber Science Inc.);

465   and a particle detector (Abakus, Klotz) was used for measuring insoluble dust particle concentrations

466   and size distribution[57]. Effective depth resolution typically was better than 20 mm. Measurements

467   were exactly synchronized in depth using a multicomponent standard solution; the accuracy of the

468   depth assignment for all measurements typically was better than 5 mm.

469   **High-resolution measurements of [10]Be in ice cores using accelerator mass spectrometry (AMS).**

470   Samples from the NEEM-2011-S1, WDC, NGRIP, and TUNU2013 ice cores encompassing the time

471   period of the $\Delta^{14}C$ anomalies from tree-ring records[12,22-25] were used for [10]Be analysis

472   (Supplementary Data S1). NEEM-2011-S1 and WDC were sampled in exact annual resolution, using

473   the maxima (minima in WDC) of the annual cycles of Na concentrations to define the beginning of

474   the calendar year[16]. NGRIP was sampled at a constant resolution of 18.3 cm providing an age

475   resolution of about one year. Similarly, TUNU2013 was sampled in quasi-annual resolution according

476   to the average annual-layer thickness expected at this depth based on prior volcanic synchronization

477   to NEEM-2011-S1. The relative age uncertainty for TUNU2013 with respect to the dependent NEEM-

478   2011-S1 chronology at this depth is assumed to be ±1 year at most given a distinctive match for

479   selected volcanic trace elements in both ice core records (752-764 CE, NS1-2011 timescale). Sample

480   masses ranged between 100 and 450 g, resulting in median overall quantification uncertainties of

481   less than 4–7%. The [10]Be/[9]Be ratios of samples and blanks were measured relative to well-

482   documented [10]Be standards[13] by AMS at Purdue's PRIME laboratory (WDC, NEEM-2011-S1,

483   Tunu2013) and Uppsala University (NGRIP)[58,59]. Results were corrected for an average blank [10]Be/[9]Be

484   ratio, corresponding to corrections of 2–10% of the measured [10]Be/[9]Be ratios.

485   **Annual-layer dating using the StratiCounter algorithm.** For annual-layer interpretation, we used

486   DRI's broad-spectrum aerosol concentration data from WDC (188–577 m), NEEM-2011-S1 (183–411

487 m), and NEEM (410–515 m), as well as NEEM aerosol concentration data (183–514 m) from the field-

488 based CFA system. The original timescale for NEEM-2011-S1 was based on volcanic synchronization

489 to the NGRIP sulfate record on the GICC05 timescale and annual-layer interpretation between the

490 volcanic age markers, while WDC previously was dated by annual-layer counting[16].

491 Parameters with strong intra-annual variability included tracers of sea salt (e.g., Na, Cl, Sr),

492 dust (e.g., Ce, Mg, insoluble particle concentration), and marine biogenic emissions such as non-sea-

493 salt sulfur (nssS). Tracers of biomass-burning emissions, such as BC, NH_4^+, and NO_3^-, also showed

494 strong seasonal variations in deposition during pre-industrial times[16,60,61]. Datasets used for annual

495 layer interpretation are provided in Extended Data Table 1. For NEEM-2011-S1, the final database

496 used for annual-layer dating included 13 parameters and the ratio of nssS/Na. For WDC, the final

497 database included five parameters and the ratio of nssS/Na. For NEEM (410-515 m depth), the final

498 database included eight parameters (Na^+, Ca^{2+}, NH_4^+, H_2O_2, NO_3^-, conductivity, insoluble particle

499 concentrations, and ECM[62]) from the field-based measurements and eleven parameters (Na, Cl, Mg,

500 Mn, Sr, nssS, nssS/Na, nssCa, BC, NO_3^-, NH_4^+) from the DRI system.

501 We focused here on the time period prior to the large volcanic eruption of Samalas in 1257

502 CE[31], clearly detectable as an acidic peak in both ice-core records, and consequently started annual-

503 layer counting of NEEM-2011-S1, NEEM, and WDC at the depth of the corresponding sulfur signal.

504 For the time period 1257 CE to present, ice-core chronologies were constrained by numerous

505 historic eruptions and large sulfate peaks showing a strong association to Northern Hemisphere (NH)

506 cooling events as indicated by tree-ring records[16].

507 We applied the StratiCounter layer-detection algorithm[32] to the multi-parameter aerosol

508 concentration records (n=14 for NEEM-2011-S1; n=6 for WDC; n=8 for NEEM <410 m; n=19 for NEEM

509 >410 m) to objectively determine the most likely number of annual layers in the ice cores along with

510 corresponding uncertainties. The StratiCounter algorithm is based on statistical inference in Hidden

511 Markov Models (HMMs), and it determines the maximum likelihood solution based on the annual

512 signal in all aerosol records in parallel. Some of these displayed a high degree of similarity, so we

513 weighted these records correspondingly lower. The algorithm was run step-wise down the core,

514 each batch covering approximately 50 years, with a slight overlap. All parameters for the statistical

515 description of a mean layer and its inter-annual variability in the various aerosol records were

516 determined independently for each batch as the maximum likelihood solution. The algorithm

517 simultaneously computes confidence intervals for the number of layers within given sections,

518 allowing us to provide uncertainty bounds on the number of layers between selected age-marker

519 horizons (Extended Data Table 2).

520 Annual-layer detection in the NEEM main core below 410 m was made more difficult by

521 frequent occurrence of small gaps in the two independent high-resolution aerosol data sets.

522 Depending on the parameter, data gaps from the CFA field measurements accounted for up to 20%

523 of the depth range between 410 and 515 m, but the combined aerosol records from both analyses

524 provided an almost complete aerosol record with 96% data coverage. As this was the first time that

525 the StratiCounter algorithm was used simultaneously on data records from two different melt

526 systems, with different characteristics and lack of exact co-registration, we also manually

527 determined annual layers below 410 m using the following approaches: one investigator used Na

528 and nssCa concentrations and the ratio of nssS/Na (from DRI analysis) as well as Na^+ and insoluble

529 particle concentrations (from CFA analysis) as primary dating parameters. BC, NH_4^+, nssS, and

530 conductivity were used as secondary dating parameters where annual-layer interpretation was

531 ambiguous. A second investigator used DRI's Na, Ca, BC, NH_4^+ and CFA Na^+, Ca^{2+}, and NH_4^+

532 measurements as parameters. The annual-layer interpretation of the NEEM core between 410 and

533 514 m from investigator 1 was within the interpretation uncertainties of the StratiCounter output,

534 from which it differed less than a single year over the majority of this section, and it differed from

535 independently counted timescales (e.g., GICC05)[62] by on average less than three years (Extended

536 Data Fig. 2). This set of layer counts was used for the resulting timescale.

537 **New ice-core chronologies (NS1-2011, WD2014).** We defined the depth of NEEM-2011-S1

538 containing the maximum [10]Be concentration as the year 775 CE. Relative to this constraint, the

539 maximum likelihood ages for three large volcanic sulfate peaks were within ±1 year of documented

540 historical reports from early written sources of prominent and sustained atmospheric dimming

541 observed in Europe and/or the Near East (Extended Data Table 3, Supplementary Data S2).

542 Automated-layer identification for NEEM-2011-S1 was therefore constrained by tying the respective

543 ice-core volcanic signals to the corresponding absolute historically-dated ages of 536, 626, and 939

544 CE (Extended Data Table 2) – thereby creating a new ice-core timescale (NS1-2011). The volcanic

545 sulfur signal corresponding to the eruption of Samalas believed to have occurred in late 1257[31] was

546 constrained to 1258 CE to account for several months' delay in sulfate deposition in the high

547 latitudes. Before 86 CE (the bottom depth of NEEM-2011-S1), the NS1-2011 timescale was extended

548 using the manually-derived annual-layer interpretation of the combined NEEM aerosol data-sets

549 back to 500 BCE (Fig. 2).

550 In NS1-2011 we did not attribute acid layers to the historical eruptions Vesuvius 79 and

551 Hekla 1104, due to a lack of corroborative tephra at these depths in this and a previous study[63].

552 Possible Vesuvian tephra was reported from the Greenland Ice Sheet Project (GRIP) ice core at 429.3

553 m depth[64], but in view of the new annual-layer dating results (Extended Data Fig. 3), we concluded

554 that this layer dates to 87/88 CE. Furthermore, volcanic sulfate deposition values for the

555 corresponding event show a strong spatial gradient over Greenland with highest values in NW

556 Greenland[16] and lowest in Central and South Greenland[65], favoring the attribution of a volcanic

557 source from the high latitudes. Documentary sources (Supplementary Data S2) also suggest that the

558 main vector of ash transport following the Vesuvius 79 CE eruption was toward the eastern

559 Mediterranean[66].

560 For WDC, we do not have other sufficiently well-determined age constraints besides the

561 rapid [10]Be increase in 775 CE and the sulfur signal of the Samalas 1257 eruption. Therefore, no

562   additional constraints were used when creating the new ice-core timescale ("WD2014") from the

563   StratiCounter annual-layer interpretation back to 396 BCE.

564   Depth-age information for six distinctive marker horizons in Greenland is given, and five of

565   these horizons were used to constrain NS1-2011 (Extended Data Table 3). Similarly, depth

566   information, the number of annual layers, and 95% confidence intervals between distinctive volcanic

567   marker horizons are given for NEEM, NEEM-2011-S1, and WDC, supporting attribution of these ice-

568   core signals to eruptions in the low latitudes with bipolar sulfate deposition.

569   **Evaluation of NS1-2011 using independent age information.** We evaluated timescale accuracy using

570   additional distinctive age markers not used during chronology development:

571   1) Tephra from the eruption of Changbaishan/Tianchi (China)[67] was detected in NEEM-2011-S1

572   in 946–947 CE, in agreement with widespread documentary evidence of an eruption in that

573   region in winter 946/47 CE[68] also supported by a high-precision ^{14}C wiggle-match age of 946 ±

574   3 CE obtained from a tree killed during this eruption[68].

575   2) The rapid increase of ^{10}Be from the 994 event occurred in NEEM-2011-S1 in 993 CE,

576   consistent with Δ^{14}C from Japanese tree rings showing that the rapid increase in

577   radionuclide production took place between the NH growing seasons of 993 and 994 CE[23].

578   3) To assess the accuracy of the NS1-2011 timescale prior to the earliest age marker at 536 CE,

579   we compiled an independent time series of validation points, featuring years with well dated

580   historical reports of atmospheric phenomena associated with high-altitude volcanic dust

581   and/or aerosols (Supplementary Data S2) as known from modern observations to occur after

582   major eruptions (e.g., Krakatau, 1883). These phenomena include diminished sunlight,

583   discoloration of the solar disk, solar coronae (i.e., Bishop's Rings), and deeply red twilights

584   (i.e., volcanic sunsets)[69,70]. Thirty-two events met our criteria as validation points for the pre-

585   536 CE NS1-2011 timescale. For the earliest in 255 BCE, it was reported in Babylon that "the

586   disk of the sun looked like that of the moon"[73]. For the latest in 501 CE, it was reported in

587   North China that "the Sun was red and without brilliance"[74]. We found that NEEM volcanic

588   event years (including both NEEM and NEEM-2011-S1 data) occurred closely in time (i.e.,

589   within a conservative ±3 year margin) to 24 (75.0%) of our validation points (Extended Data

590   Figure 2). To assess whether this association arose solely by chance, we conducted a Monte

591   Carlo equal means test with 1,000,000 iterations (Supplementary Data S2) and found that

592   the number of volcanic event years within ±3 years of our validation points was significantly

593   greater than expected randomly (p<0.001). A significant association was also observed

594   (p<0.001) when using less conservative error margins (±1 and ±2 years) and when excluding

595   any historical observations with less certainty of a volcanic origin (Supplementary Data S2).

596   When placing volcanic event years on the original GICC05 timescale, we did not observe any

597   statistically significant association with our independent validation points.

598   **Potential causes of a previous ice-core dating bias.** Interpretation of annual layers in ice cores is

599   subject to accumulating age uncertainty due to ambiguities in the underlying ice-core profiles[30,73].

600   Bias in existing chronologies may arise from several factors, including: 1) low effective resolution of

601   some ice core measurements (NGRIP, GRIP); 2) use of only single (or few) parameters for annual-

602   layer interpretation (GRIP, Dye-3); 3) intra-annual variations in various ice-core parameters falsely

603   interpreted as layer boundaries (e.g., caused by summer melt in Dye-3)[74]; 4) use of tephra believed

604   to originate from the 79 CE Vesuvian eruption[64] as a fixed reference horizon to constrain the

605   Greenland ice-core dating[30]; 5) use of manual-layer interpretation techniques that may favor

606   interpretations consistent with *a priori* knowledge or existing chronologies (WDC)[16,21].

607   **Volcanic synchronization of B40, TUNU2013, and NGRIP to WDC and NEEM.** Two high-resolution

608   sulfur ice-core records (TUNU2013, Greenland and B40, Antarctica) were synchronized to NEEM-

609   2011-S1 and WDC, respectively, using volcanic stratigraphic age markers[17] with relative age

610   uncertainty between the tie-points estimated to not exceed ±2 years. The NGRIP sulfate record

611   measured at 5 cm depth resolution[15] similarly was synchronized to NS1-2011 using 124 volcanic tie-

612   points between 226 and 1999 CE. During the time period with no sulfur record yet available for WDC

613   (before 396 BCE), a tentative chronology for B40 was derived by linearly extrapolating mean annual-

614   layer thickness for B40 as derived from the synchronization to WDC between the earliest volcanic

615   match points.

616   **2,500 year global volcanic forcing ice-core index.** We constructed an index of global volcanic aerosol

617   forcing by (1) re-dating and extending to 500 BCE an existing reconstruction of sulfate flux from an

618   Antarctic ice-core array[17] by applying an area weighting of 80/20 between East Antarctica and West

619   Antarctica to B40 and WDC volcanic sulfate flux values, respectively; (2) compositing NGRIP and the

620   NEEM-2011-S1/NEEM sulfate flux records to a similar Greenland sulfate deposition composite back

621   to 500 BCE; (3) using established scaling functions[6,75] to estimate hemispheric sulfate aerosol loading

622   from both polar ice-core composites; and (4) scaling global aerosol loading to the total (i.e., time

623   integrated) radiative volcanic aerosol forcing following the Tambora 1815 eruption[7]. Since the NS1-

624   2011 and WD2014 timescales are independent of each other, the timing of bipolar events had to be

625   adjusted to follow a single timescale to derive a unified global volcanic forcing series. We chose NS1-

626   2011 as the reference chronology for most of the volcanic time series because this age model was

627   constrained and validated by more stratigraphic age markers than WD2014. WD2014 was used as

628   the reference chronology only between 150 and 450 CE, because of better data quality during that

629   time period. TUNU2013 was not included in the Greenland ice-core composite because annual-layer

630   thickness variability at this site is influenced strongly by glaciological processes, leading to relatively

631   large uncertainties in atmospheric sulfur-deposition determinations.

632   **NH tree-ring composite.** Tree-ring records from certain locations reflect summer cooling (as is

633   widespread observed after volcanic eruptions) with no age uncertainty in annual ring-width dating,

634   thus allowing independent validation of ice-core timescales and the derived volcanic forcing indices.

635   However, no tree-ring-based temperature reconstructions of large spatial scales span the full 2,500

636   years represented by our new ice-core chronologies. To thus evaluate our new ice-core chronologies

637   and assess the consistency of response throughout the past 2,500 years, we compiled a composite

638   (entitled "N-Tree") of multi-centennial tree growth records at locations where temperature is the

639   limiting growth factor. We selected available NH tree-ring records that provided a continuous record

640   of >1,500 years and showed a significant positive relationship with JJA temperatures during the

641   instrumental period (1901–2000 CE) with p<0.005 (adjusted for a reduced sample size due to

642   autocorrelation of the datasets). In total, five tree-ring chronologies (three based on ring-width

643   measurements, two based on measurements of maximum latewood density) met these

644   criteria[42,43,76-78] of which three are located in the high-latitudes of Eurasia (Extended Data Figure 1).

645   As various climatic and non-climatic parameters may influence sensitivity of tree growth to

646   temperatures during the 20th century[79-81], we used the time period 1000-1099 CE as a common

647   baseline for standardizing tree growth anomalies among the five chronologies and built a tree

648   growth composite record "N-Tree" (z-scores) by averaging the individual records. Correlations

649   between "N-Tree" (N=5) and the average of three regional reconstructions for the Arctic, Europe,

650   and Asia (N>275)[3] between 1800 and 2000 CE are very high (r = 0.86, N=201, p<0.0001), suggesting

651   that much of the large-scale variation in temperature is explained by these selected tree-ring

652   records. Three records in "N-Tree" cover the period from 138 BCE to the present, thus allowing at

653   least a qualitative assessment of the coherence of growth reduction following large volcanic

654   eruptions prior to the Common Era (Fig. 2, Extended Data Fig. 4).

655   **Temperature reconstructions.** To quantify the CE climate impact and investigate regional

656   differences, we used tree-ring-based JJA temperature reconstructions covering the past 2,000 years

657   with demonstrated strong relationship (r ≥ 0.45; p<0.0001; Extended Data Fig. 1) to instrumental JJA

658   temperature data[82] between 1901 and 2000. For regions where this criterion was met by several

659   reconstructions (e.g., Scandinavia), we limited the analysis to the most recently updated

660   reconstruction[35]. Three regional reconstructions from Central Europe [42], Northern Europe[35], and

661   Northern Siberia (Yamal, not shown)[76] as well as a continental-scale reconstruction for Europe[3] met

662   this criterion and were used to quantify the average response of summer temperature to volcanic

663   forcing during the Common Era (Figs. 3, 4).

664 **Superposed epoch analyses.** To assess tree-ring growth reduction and summer cooling following

665 large eruptions, we used superposed epoch analyses[83,84]. We selected all volcanic eruptions (28

666 events in total, 24 CE events) with time-integrated volcanic forcing greater than -7.5 W m^{-2} (i.e.,

667 eruptions larger than Pinatubo 1991) and aligned the individual segments of "N-Tree" and regional

668 JJA temperature reconstructions relative to ice-core-indicated peak forcing. Composite response was

669 calculated for the average of the individual series (lag 0 to lag 10 or 15 years) relative to the average

670 values five years prior to individual volcanic events (lag -5 to lag -1 year). 95% confidence intervals

671 represent 2 SEM of the tree-growth (Extended Data Figure 4) and temperature anomalies (Figure 4)

672 associated with the multiple eruptions.

673 **Cryptotephra analyses of the 536 CE sample from NEEM-2011-S1.** We analyzed samples from

674 NEEM-2011-S1 for tephra between 326.73 and 328.06 m depth, corresponding to 531–539 CE (NS1-

675 2011 timescale). Samples (200 to 500 g) were filtered, and elemental composition of recovered

676 volcanic glass shards determined by electron microprobe analysis (EPMA) at Queen's University

677 Belfast using established protocols[63,67,85] and secondary glass standards[86,87]. Between 326.73 and

678 327.25 m, large volume samples were cut at 8 cm depth resolution (≤0.5 yr) and with an average

679 cross section of 26 cm^2. Between 327.25 and 328.06 m, the average cross section was 7 cm^2 and

680 depth resolution 20 cm (~1 yr resolution). Tephra particles (n ≥17) were isolated from a sample of ice

681 (327.17–327.25 m depth, 251 g) corresponding to the sulfate spike at 536 CE. The glass shards were

682 heterogeneous in size (20–80 μm), morphology (platey, blocky, vesicular, microlitic), and

683 geochemistry (andesitic, trachytic, rhyolitic). Individual shards had geochemical compositions that

684 share affinities with volcanic systems in the Aleutian arc (Alaska)[88], Northern Cordilleran volcanic

685 province (British Columbia)[89], and Mono-Inyo Craters area (California)[90,91] – indicating at least three

686 synchronous eruptive events, all situated in western North America between 38 and 58°N (Extended

687 Data Fig. 5; Supplementary Data S5).

688 **Data:** Ice-core data (chemistry, including sulfur; [10]Be), resulting timescales, and the volcanic forcing

689 reconstruction are provided as online supplementary material (Supplementary Data S1, S3-S5);

690 Historical documentary data is provided as Supplementary Data S2. The code for the StratiCounter

691 program is accessible at the github repository (http://www.github.com/maiwinstrup/StratiCounter);

692 NGRIP SO_4 data can be obtained at http://www.iceandclimate.nbi.ku.dk/data/2012-12-

693 03_NGRIP_SO4_5cm_Plummet_et_al_CP_2012.txt ; tree-ring records and temperature

694 reconstructions are from Pages-2k Consortium (Database S1, S2)

695 (http://www.nature.com/ngeo/journal/v6/n5/full/ngeo1797.html#supplementary-information).

696 **References**

697 50   Dahl-Jensen, D. *et al.* Eemian interglacial reconstructed from a Greenland folded ice core.

698   *Nature* **493**, 489-494 (2013).

699 51   McConnell, J. R. Continuous ice-core chemical analyses using inductively Coupled Plasma

700   Mass Spectrometry. *Environ Sci Technol* **36**, 7-11 (2002).

701 52   McConnell, J. R. & Edwards, R. Coal burning leaves toxic heavy metal legacy in the Arctic. *P

702   Natl Acad Sci USA* **105**, 12140-12144 (2008).

703 53   Pasteris, D. R. *et al.* Seasonally resolved ice core records from West Antarctica indicate a sea

704   ice source of sea-salt aerosol and a biomass burning source of ammonium. *J Geophys Res-

705   Atmos* **119**, 9168-9182 (2014).

706 54   Abram, N. J., Mulvaney, R. & Arrowsmith, C. Environmental signals in a highly resolved ice

707   core from James Ross Island, Antarctica. *J Geophys Res-Atmos* **116**, D20116, doi:

708   10.1029/2011jd016147 (2011).

709 55   Kaufmann, P. R. *et al.* An Improved Continuous Flow Analysis System for High-Resolution

710   Field Measurements on Ice Cores. *Environ Sci Technol* **42**, 8044-8050 (2008).

711 56   Bigler, M. *et al.* Optimization of High-Resolution Continuous Flow Analysis for Transient

712   Climate Signals in Ice Cores. *Environ Sci Technol* **45**, 4483-4489 (2011).

713   57   Ruth, U., Wagenbach, D., Steffensen, J. P. & Bigler, M. Continuous record of microparticle

714   concentration and size distribution in the central Greenland NGRIP ice core during the last

715   glacial period. *J Geophys Res-Atmos* **108**, doi: 10.1029/2002jd002376 (2003).

716   58   Woodruff, T. E., Welten, K. C., Caffee, M. W. & Nishiizumi, K. Interlaboratory comparison of

717   Be-10 concentrations in two ice cores from Central West Antarctica. *Nucl Instrum Meth B*

718   **294**, 77-80 (2013).

719   59   Berggren, A. M. *et al.* Variability of Be-10 and delta O-18 in snow pits from Greenland and a

720   surface traverse from Antarctica. *Nucl Instrum Meth B* **294**, 568-572 (2013).

721   60   Bisiaux, M. M. *et al.* Changes in black carbon deposition to Antarctica from two high-

722   resolution ice core records, 1850-2000 AD. *Atmos Chem Phys* **12**, 4107-4115 (2012).

723   61   Pasteris, D., McConnell, J. R., Edwards, R., Isaksson, E. & Albert, M. R. Acidity decline in

724   Antarctic ice cores during the Little Ice Age linked to changes in atmospheric nitrate and sea

725   salt concentrations. *J Geophys Res-Atmos* **119**, 5640-5652 (2014).

726   62   Rasmussen, S. O. *et al.* A first chronology for the North Greenland Eemian Ice Drilling (NEEM)

727   ice core. *Clim Past* **9**, 2713-2730 (2013).

728   63   Coulter, S. E. *et al.* Holocene tephras highlight complexity of volcanic signals in Greenland ice

729   cores. *J Geophys Res-Atmos* **117**, D21303, doi: 10.1029/2012jd017698 (2012).

730   64   Barbante, C. *et al.* Greenland ice core evidence of the 79 AD Vesuvius eruption. *Clim Past* **9**,

731   1221-1232 (2013).

732   65   Clausen, H. B. *et al.* A comparison of the volcanic records over the past 4000 years from the

733   Greenland Ice Core Project and Dye 3 Greenland Ice Cores. *J Geophys Res-Oceans* **102**,

734   26707-26723 (1997).

735   66   Rolandi, G., Paone, A., Di Lascio, M. & Stefani, G. The 79 AD eruption of Somma: The

736   relationship between the date of the eruption and the southeast tephra dispersion. *J*

737   *Volcanol Geoth Res* **169**, 87-98 (2008).

738   67   Sun, C. Q. *et al.* Ash from Changbaishan Millennium eruption recorded in Greenland ice:

739   Implications for determining the eruption's timing and impact. *Geophys Res Lett* **41**, 694-701

740   (2014).

741   68   Xu, J. D. *et al.* Climatic impact of the Millennium eruption of Changbaishan volcano in China:

742   New insights from high-precision radiocarbon wiggle-match dating. *Geophys Res Lett* **40**, 54-

743   59 (2013).

744   69   Deirmendjian, D. On volcanic and other particulate turbidity anomalies. *Advances in*

745   *Geophysics* **16**, 267-296 (1973).

746   70   Vollmer, M. Effects of absorbing particles on coronas and glories. *Appl Optics* **44**, 5658-5666

747   (2005).

748   71   Sachs, A. J. & Hunger, H. Astronomical diaries and related texts from Babylonia. Volume 3:

749   Diaries from 164 B.C. to 61 B.C. Wien: Verlag der Österreichischen Akademie der

750   Wissenschaften (1996).

751   72   Wittmann, A. D. & Xu, Z. T. A Catalog of Sunspot Observations from 165 Bc to Ad 1684.

752   *Astron Astrophys Sup* **70**, 83-94 (1987).

753   73   Rasmussen, S. O. *et al.* A new Greenland ice core chronology for the last glacial termination.

754   *J Geophys Res-Atmos* **111**, D06102 doi: 10.1029/2005jd006079 (2006).

755   74   Herron, M. M., Herron, S. L. & Langway, C. C. Climatic Signal of Ice Melt Features in Southern

756   Greenland. *Nature* **293**, 389-391 (1981).

757   75   Gao, C. H., Oman, L., Robock, A. & Stenchikov, G. L. Atmospheric volcanic loading derived

758   from bipolar ice cores: Accounting for the spatial distribution of volcanic deposition. *J*

759   *Geophys Res-Atmos* **112**, D09109, doi: 10.1029/2006jd007461 (2007).

760   76   Briffa, K. R. *et al.* Reassessing the evidence for tree-growth and inferred temperature change

761   during the Common Era in Yamalia, northwest Siberia. *Quaternary Sci Rev* **72,** 83-107 (2013).

762 77 Grudd, H. Tornetrask tree-ring width and density AD 500-2004: a test of climatic sensitivity

763   and a new 1500-year reconstruction of north Fennoscandian summers. *Clim Dynam* **31**, 843-

764   857 (2008).

765 78 Salzer, M. W., Bunn, A. G., Graham, N. E. & Hughes, M. K. Five millennia of

766   paleotemperature from tree-rings in the Great Basin, USA. *Clim Dynam* **42**, 1517-1526

767   (2014).

768 79 McMahon, S. M., Parker, G. G. & Miller, D. R. Evidence for a recent increase in forest growth.

769   *P Natl Acad Sci USA* **107**, 3611-3615 (2010).

770 80 Salzer, M. W., Hughes, M. K., Bunn, A. G. & Kipfmueller, K. F. Recent unprecedented tree-

771   ring growth in bristlecone pine at the highest elevations and possible causes. *P Natl Acad Sci*

772   *USA* **106**, 20348-20353 (2009).

773 81 Briffa, K. R. *et al.* Reduced sensitivity of recent tree-growth to temperature at high northern

774   latitudes. *Nature* **391**, 678-682 (1998).

775 82 Rohde, R. *et al.* A New Estimate of the Average Land Surface Temperature Spanning 1753 to

776   2011. *Geoinfor Geostat: An Overview* **1**, doi: 10.4172/2327-4581.1000101 (2013).

777 83 Mass, C. F. & Portman, D. A. Major volcanic eruptions and climate: A critical evaluation. *J.*

778   *Climate* **2,** 566-593.

779 84 Fritts, H. C., Lofgren, G. R. & Gordon, G. A. Variations in Climate since 1602 as Reconstructed

780   from Tree Rings. *Quaternary Res* **12**, 18-46 (1979).

781 85 Jensen, B. J. L. *et al.* Transatlantic distribution of the Alaskan White River Ash. *Geology* **42**,

782   875-878 (2014).

783 86 Oskarsson, N., Sigvaldason, G. E. & Steinthorsson, S. A Dynamic-Model of Rift-Zone

784   Petrogenesis and the Regional Petrology of Iceland. *J Petrol* **23**, 28-74 (1982).

785 87 Kuehn, S. C., Froese, D. G., Shane, P. A. R. & Participants, I. I. The INTAV intercomparison of

786   electron-beam microanalysis of glass by tephrochronology laboratories: Results and

787   recommendations. *Quatern Int* **246**, 19-47 (2011).

788   88   Kaufman, D. S. *et al.* Late Quaternary tephrostratigraphy, Ahklun Mountains, SW Alaska. *J*

789   *Quaternary Sci* **27**, 344-359 (2012).

790   89   Lakeman, T. R. *et al.* Holocene tephras in lake cores from northern British Columbia, Canada.

791   *Can J Earth Sci* **45**, 935-947 (2008).

792   90   Bursik, M., Sieh, K. & Meltzner, A. Deposits of the most recent eruption in the Southern

793   Mono Craters, California: Description, interpretation and implications for regional marker

794   tephras. *J Volcanol Geoth Res* **275**, 114-131 (2014).

795   91   Sampson, D. E. & Cameron, K. L. The Geochemistry of the Inyo Volcanic Chain - Multiple

796   Magma Systems in the Long Valley Region, Eastern California. *J Geophys Res-Solid* **92**, 10403-

797   10421 (1987).

798   92   Veres, D. *et al.* The Antarctic ice core chronology (AICC2012): an optimized multi-parameter

799   and multi-site dating approach for the last 120 thousand years. *Clim Past* **9**, 1733-1748

800   (2013).

801   93   Siebert, L., Simkin, T. & Kimberly, P. *Volcanoes of the World*. 3rd edn, University of California

802   Press (2010).

803

804   **Extended Data Figure 1 | Location of study sites. a)** Map showing locations of the five ice-cores

805   (WDC, B40, NEEM, NGRIP and TUNU) used in this study. Sites of temperature-limited tree-ring

806   chronologies (green) [42,43,76-78] and sites with annual Δ^{14}C measurements from tree-rings in the 8th

807   century CE (red outline) are marked; **b)** metadata for the ice cores, tree-ring chronologies and

808   temperature reconstructions used.

809   **Extended Data Figure 2 | Volcanic dust veils from historical documentary sources in relation to**

810   **NEEM.** Time series of 32 independently-selected chronological validation points from well-dated

811   historical observations of atmospheric phenomena with known association to explosive volcanism

812   (e.g., diminished sunlight, discolored solar disk, solar corona or Bishop's Ring, red volcanic sunset) as

813   reported in the Near East, Mediterranean region, and China, prior to our earliest chronological age

814   marker at 536 CE. Black lines represent the magnitude (scale on vertical y-axes) of annual sulfate

815   deposition measured in NEEM (NEEM and NEEM-2011-S1 ice cores) from explosive volcanic events

816   on the new NS1-2011 timescale. Red crosses depict the 24 (75%) historical validation points for

817   which NEEM volcanic events occur within a conservative ±3 year uncertainty margin. Blue crosses

818   represent the eight points for which volcanic events are not observed. The association between

819   validation points and volcanic events is statistically significantly non-random at >99.9% confidence.

820   **Extended Data Figure 3 | Timescale comparison.** Age differences of the timescales **a)** NS1-2011 and

821   GICC05 for the NEEM-2011-S1/NEEM ice cores and **b)** WD2014 and WDC06A-7 for WDC. Differences

822   before 86 CE (the bottom age of NEEM-2011-S1) deriving from the annual-layer counting of the

823   NEEM core are shown for major volcanic eruptions relative to the respective signals in NGRIP on the

824   annual-layer counted GICC05 timescale. Marker events used for constraining the annual-layer dating

825   (solid line) and for chronology evaluation (dashed lines) are indicated. Triangles mark volcanic

826   signals. Also indicated is the difference between WD2014 and the Antarctic ice-core chronology

827   (AICC2012)[92], based on volcanic synchronization between the WDC and EDC96 ice cores.

828   **Extended Data Figure 4 | Post-volcanic suppression of tree growth.** Superposed epoch analysis for

829   large volcanic eruptions using the **a)** 28 largest volcanic eruptions; **b)** 23 largest tropical eruptions; **c)**

830   five largest NH eruptions; and **d)** eruptions larger than Tambora 1815 with respect to sulfate aerosol

831   loading. Shown are growth anomalies of a multi-centennial tree-ring composite record (N-Tree) 15

832   years after the year of volcanic sulfate deposition, relative to the average of five years before the

833   events. Dashed lines indicate 95% confidence intervals (2 SEM) of the tree-ring growth anomalies

834   associated with the multiple eruptions.

835   **Extended Data Figure 5 | Major element composition for ice core tephra QUB-1859 and reference**

836   **material.** Shown are selected geochemistry data: (**a)** SiO_2 vs. total alkali ($K_2O + Na_2O$); **b)** FeO (total

837   iron oxides) vs. TiO_2; **c)** SiO_2 vs. Al_2O_3; and **d)** CaO vs. MgO) from 11 shards extracted from the NEEM-

838   2011-S1 ice core between 327.17 and 327.25 m depth, representing the age range 536.0–536.4 CE

839   on the new, NS1-2011 timescale. Data for Late Holocene tephra from Mono Craters (California) are

840   from the compilation by ref. 90 (all references in Methods); data for Aniakchak (Alaska) are from

841   reference material published by ref. 88; and data for the early Holocene upper Finlay tephra ,

842   believed to be from the Edziza complex in the Upper Cordilleran Volcanic province (British

843   Columbia), are from ref. 89.

844   **Extended Data Table 1 | Ice-core dating.** Parameters used for annual-layer interpretation.

845   Parameters measured by the CFA system in the field are underlined. Stratigraphic age marker used

846   to constrain annual-layer counting (*) and horizons used to evaluate the timescale (†).

847   **Extended Data Table 2 | Annual-layer results using the StratiCounter program.** Maximum-

848   likelihood number of annual layers and confidence intervals derived from annual-layer counting

849   between distinctive marker horizons and corresponding ages relative to the 775 CE [10]Be event.

850   *UE: Unattributed volcanic signal and year of sulfate deposition based on final age models (negative

851   numbers are Year BCE).

852   †Year (BCE/CE) calculated from the number of annual layers relative to the fixed age marker in 775

853   CE.

854   ‡Depth has been estimated from the average depth offset between NEEM-2011-S1 and NEEM.

855   §Fixed age marker based on the 10Be maximum annual value.

856 ||Section with 6 m gap in the NEEM 2011-S1 core DRI data (this section is not used for calculating

857   average age).

858   ¶ This section is based on the NEEM field CFA data, since the DRI data does not cover the entire

859   interval.

860   # Section is based on combined data set of DRI and field-measured CFA data. The number of annual

861   layers in this section from manual interpretation by investigator 1 was 383 (±7), and that of

862   investigator 2 was 393 (±8) layers. Most of the difference between the three layer counts was

863   occurring below 480 m (i.e., before 300 BCE), where data gaps were more frequent.

864   ☆Independent age markers used to constrain annual-layer dating in a second iteration to derive the

865   final ice-core age model NS1-2011.

866   **Tephra particles were extracted from the depth range 327.17–327.25 m depth (see

867   Supplementary Data).

868   ††Unattributed volcanic signal that was previously attributed to the historic 79 CE eruption of

869   Vesuvius[64].

870   **Extended Data Table 3 | Historical documentary evidence for key volcanic eruption age markers**

871   **536-939 CE.** A comprehensive list of all sources, including translations and assessment of the

872   confidence placed in each source and its chronological information is given in Supplementary Data.

873   **Extended Data Table 4 | Large volcanic eruptions during the past 2,500 years.** Years with negative

874   numbers are before the Common Era (BCE). Tentative attribution of ice-core signals to historic

875   volcanic eruptions is based on the Global Volcanism Program volcanic eruption database[93]. Average

876   (summer) temperature for the associated cold year is given for the average of Europe and the

877   Arctic[3].

878   *Total global aerosol forcing was estimated by scaling total sulfate flux from both polar ice sheets to

879   the reconstructed total (i.e., time integrated) aerosol forcing for Tambora 1815[7] (Methods); for high

880   latitude NH eruptions, Greenland fluxes were scaled by a factor of 0.57[6].

881   † Unattributed volcanic events (UE) and tentative attributions for non-documented historic

882   eruptions (?) are marked.

883   **Extended Data Table 5 | Post-volcanic cooling.** Coldest years and decades (1–2000 CE, JJA

884   temperature wrt. 1901–2000) for Europe[3] and years (500 BCE–1250 CE) and decades (500 BCE–2000

885   CE) with strong growth reduction in the N-Tree composite(wrt. 1000–1099). Ages of the volcanic

886   events from the ice cores reflect the start of volcanic sulfate deposition in Greenland (NS1-2011

887   timescale) with the largest 40 events indicated in bold letters and tropical eruptions underlined.

888   Years with negative numbers are before the Common Era (BCE).

889   * Latewood frost ring in bristlecone pines within ±1 year[34].

a 1250 - 2000 CE
   10 largest eruptions

   +7 yr

   78 - 1000 CE
   7 largest eruptions

b Year (CE) original ice core dating

   WDC
   (Antarctica)

   +7 yr

   TUNU2013
   (Greenland)

   +7 yr

   NGRIP
   (Greenland)

   NEEM
   2011-S1
   (Greenland)

   +7 yr

   Oak (Germany)
   Cedar (Japan)

   775 Event

c Year (CE) original ice core dating

   NEEM
   2011-S1
   (Greenland)

   +7 yr

   Cedar (Japan)

   994 Event

Greenland

NEEM   NEEM-2011-S1

-426
-246 -168 -146   -44   88
168   263
432
536* 626* 540 574 682 775* 939* 993 1108 1171 1231 1258*

★ Tianchi tephra (946/47)

N-Tree

-425   -43   536 540-547 574 627 940 1109

b N=18 N=10

-500-1250 CE
1250-2000 CE

-5   0   5   10
Yrs relative to ice core signal

Antarctica   WDC   B40

-430
-248 -172 -150 -47   169 266   434 540 575 682 775*   1109 1171 1230 1258*

-500 -300 -100 100 300 500 700 900 1100 1300
Year (BCE/CE)